Subpixel Alignment of MRI Data Under Cartesian and Log-Polar Sampling

Murat Balci,* Mais Alnasser, Hassan Foroosh
Computational Imaging Lab, University of Central Florida, Orlando, FL 32816-2362, USA

Abstract

Magnetic resonance imaging (MRI) allows numerous Fourier domain sampling schemes such as Cartesian and non-Cartesian trajectories (e.g. Polar, circular, and spherical). On the other hand, it provides directly the Fourier spectrum of the field of view (FOV) in the corresponding sampling scheme. Motivated by these characteristic features of MRI, we have developed a new scheme for direct Fourier domain registration of MRI data based on the phase difference matrix. We derive the exact relationship between the continuous and the discrete Fourier phase-difference for Cartesian or polar sampling schemes, and demonstrate that in each case the discrete phase diffence is a 2D sawtooth signal. Subpixel alignment under rotation, translation and scale variation is then established simply by counting the number of cycles of the sawtooth signal. The problem is formulated as an over-determined system of equations, and is solved by imposing a regularity constraint, using the method of Generalized Cross Validation (GCV).

1. Introduction

Repeated acquisitions of MRI images from the same patient under similar conditions is frequently used in clinical settings to compare pre- and post-contrast enhanced images, follow-up diagnosis, evaluation of treatment, and serial studies such as those used in functional neuro imaging. MRI technology on the other hand has been developed over the past decade to provide different Fourier domain sampling schemes. The latter has been partly motivated by the trade off between the reduction in the number of Fourier encoding steps and maximizing the signal to noise ratio. However, for angularly or radially undersampled projection techniques, discrete sampling produces imaging artifacts commonly known as streaking or radial aliasing [7]. These artifacts in practice hinder proper diagnosis by introducing errors in both registration and change detection. However, these aliasing effects are predominantly affecting high frequencies. Since MRI can provide direct Fourier domain imaging of the FOV, Fourier domain subpixel registration is a natural choice to provide a solution to this problem.

Motivated by these specific features of MRI, we have developed a direct Fourier domain sub-pixel registration technique under Cartesian and polar sampling. MRI data in practice represent planar slices, e.g. sagittal, axial, or coronal. As a result, inter-session MRI acquisitions are very closely approximated by a rigid 2D transformation and possible small changes in scaling [4]. Therefore, we will use this model throughout the paper. Our approach leads to a simple solution directly from the phase difference matrix in the form of an over-determined system of linear equations. We compare our method to existing closely related approaches, and show that it provides very accurate results in the presence of random noise and radial aliasing.

2 Background

In this section, we first discuss the concepts and the theory that are commonly borrowed from the continuous domain. We describe the problem for inter-image translations, since when the data are acquired in polar sampling, rotation and scaling reduce to translations.

Consider two continuous signals $f_1(x, y)$ and $f_2(x, y) = f_1(x-x_o, y-y_o)$, whose cross power spectrum (also known as the phase correlation) is given by

$$\hat{c}(u, v) = \frac{\hat{f}_1 \hat{f}_2^*}{|\hat{f}_1 \hat{f}_2^*|} = \exp(-ix_o u - iy_o v) \qquad (1)$$

where the hat sign indicates the Fourier transform, and the asterisk stands for the complex conjugate.

In other words, spatial translations lead to linear phase differences between the two signals along each frequency axis, i.e. [1]

$$\hat{\varphi}(u, v) = \angle \hat{c}(u, v) = x_o u + y_o v \qquad (2)$$

which is a planar surface through the origin. As a result, the spatial translations can be determined by inverse transform-

*This work was in part supported by an I2Lab graduate fellowship.

[1] Throughout this paper, we call $\exp(-ix_o u - iy_o v)$ the phase correlation function and $\hat{\varphi}(u, v) = \angle \hat{c}(u, v)$ the phase difference function. Similarly, their discrete counterparts are referred to as the discrete phase correlation matrix, and the discrete phase difference matrix, respectively.

The 18th International Conference on Pattern Recognition (ICPR'06)
0-7695-2521-0/06 $20.00 © 2006 IEEE

ing $\hat{c}(u,v)$, which leads a Dirac delta function centered at (x_o, y_o).

A discrete interpretation of this continuous-domain result is used in practice for image registration [1, 5], which yields very good results, and was also extended to sub-pixel registration in [2]. However, for MRI, which provides directly the Fourier spectrum of the field of view, it would be interesting from both practical and computational points of view to estimate the shifts directly in the Fourier domain. A practical solution for this problem was first proposed by Hoge [3]. His method requires a subspace approximation by Singular Value Decomposition (SVD), and unwrapping of the dominant left and right eigenvectors. We will show below that both unwrapping and subspace approximation may be unnecessary steps, since we derive an analytic model of the phase difference matrix and solve the problem by fitting the model to the noisy data.

3 Discrete Model

While the continuous model provides insight to the problem, it can be misleading for the discrete data. To demonstrate this, let us examine the phase difference function in (2). Inverse transforming this phase angle would yield

$$\begin{aligned}\varphi(x,y) &= \int_{-\infty}^{\infty}\int_{-\infty}^{\infty}(x_0u + y_ov)\exp(iux + ivy)dudv \\ &= -ix_o\frac{d\delta(x)}{dx} - iy_o\frac{d\delta(y)}{dy} \qquad (3)\end{aligned}$$

where the derivatives are understood in the distributional sense [9].

From bandlimited sampling theory and (3), it follows that the spatial domain representation of a component of the discrete phase matrix is given by

$$\varphi_{kl} = -i\frac{x_o}{\pi k}\left(2\text{sinc}\frac{\pi k}{x_o} - 2\cos\frac{\pi k}{x_o}\right) - i\frac{y_o}{\pi l}\left(2\text{sinc}\frac{\pi l}{y_o} - 2\cos\frac{\pi l}{y_o}\right) \qquad (4)$$

On the other hand, note that

$$\begin{aligned}i\varphi_{kl} &= \frac{x_o^2}{\pi k^2}\left(2\frac{\pi k}{x_o}\cos\frac{\pi k}{x_o} - 2\sin\frac{\pi k}{x_o}\right) \\ &+\pi\frac{y_o^2}{\pi l^2}\left(2\frac{\pi l}{y_o}2\cos\frac{\pi l}{y_o} - 2\sin\frac{\pi l}{y_o}\right) \qquad (5)\\ &= x_o\frac{2}{2\pi/x_o}\int_{-\frac{\pi}{x_o}}^{\frac{\pi}{x_o}} u\sin ku\ \mathrm{d}u + y_o\frac{2}{2\pi/y_o}\int_{-\frac{\pi}{y_o}}^{\frac{\pi}{y_o}} v\sin lv\ \mathrm{d}v \qquad (6)\end{aligned}$$

It can also be verified that

$$x_o\frac{2}{2\pi/x_o}\int_{-\frac{\pi}{x_o}}^{\frac{\pi}{x_o}} u\cos ku\mathrm{d}u + y_o\frac{2}{2\pi/y_o}\int_{-\frac{\pi}{y_o}}^{\frac{\pi}{y_o}} v\cos lv\mathrm{d}v = 0 \qquad (7)$$

and similarly

$$x_o\frac{2}{2\pi/x_o}\int_{-\frac{\pi}{x_o}}^{\frac{\pi}{x_o}} u\mathrm{d}u + y_o\frac{2}{2\pi/y_o}\int_{-\frac{\pi}{y_o}}^{\frac{\pi}{y_o}} v\mathrm{d}v = 0 \qquad (8)$$

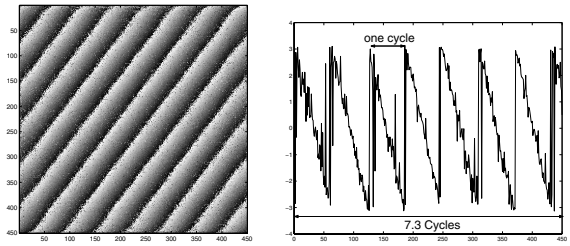

Figure 1. noisy sawtooth phase matrix corresponding to shifts of (7.3,5.6) pixels, one row of the phase difference matrix.

From (6), (7), and (8), and using the definition of the Discrete Fourier Transform (DFT) based on Fourier series [6], it follows immediately upon substituting $u = n\frac{2\pi}{N}$ and $v = m\frac{2\pi}{M}$ that φ_{kl} is a DFT coefficient of the following discrete periodic signal

$$\hat{\varphi}_{mn} = \frac{2\pi}{N}\left(x_on + j\frac{N}{x_o}\right) + \frac{2\pi}{M}\left(my_o + k\frac{M}{y_o}\right) \qquad (9)$$

where j and k are arbitrary integers.

In other words the discrete phase difference matrix for a pair of shifted images is given by $\mathbf{\Phi} = [\hat{\varphi}_{mn}]$, where $m = 0, ..., M-1$, and $n = 0, ..., N-1$. This is a discrete 2D periodic sawtooth signal as opposed to the continuous phase difference function in (2), which is a plane through the origin. Figure 1 shows examples of noisy discrete phase difference matrices. The illuminating key idea of this result is as follows: It can be verified from (9) that the periods of this discrete sawtooth signal along the two axis are given by $\left(\frac{2\pi}{x_o}, \frac{2\pi}{y_o}\right)$. In other words, there are x_o repeated cycles along each row of the phase difference matrix, where x_o may or may not be an integer. When x_o is not an integer, the number of repeated cycles in a row is given by the integer part of x_o plus a fraction of a cycle defined by the non-integer portion of x_o. A similar argument applies to the columns of $\mathbf{\Phi}$. This process of counting the number of cycles along the rows and columns of the phase matrix is essentially all that is required to determine the shifts. In the next two sections, we will design a linear estimator for this problem.

4 Proposed Method

As indicated above, the key to solve the problem is to find how many cycles of the discrete sawtooth phase difference fit in the range $[0, 2\pi]$ along each frequency axis. The number of cycles i.e. x_o and y_o may or may not be integer values, and are given by

$$x_o = \frac{\text{cycles}}{2\pi} = \frac{N}{2\pi}\frac{d\mathbf{\Phi}(m,n)}{dn} \qquad (10)$$

$$y_o = \frac{\text{cycles}}{2\pi} = \frac{M}{2\pi}\frac{d\mathbf{\Phi}(m,n)}{dm} \qquad (11)$$

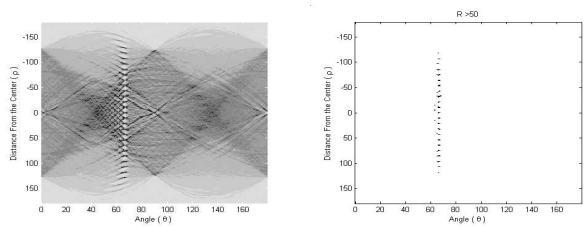

Figure 2. The Hough transform of the zero-crossings of the phase difference matrix, and the peaks detected by thresholding.

which by definition are the instantaneous frequencies. Due to noise and other sources of error, however, counting the number of cycles per 2π using equations (10) and (11) may lead to inaccurate results. To overcome this problem, we exploit the fact that a total of $M \times N$ data points are available for regression. Therefore, an accurate solution can be obtained by fitting the parameters of the analytic model to the huge data points.

The counting process visually involves detecting the set of points where the sawtooth signal takes a given value (e.g. zero) along each row or column. Algebraically this is equivalent to solving

$$n \cos\theta + m \sin\theta + \rho = 0 \tag{12}$$

where $\tan\theta = \frac{N y_o}{M x_o}$ and $\rho = k\frac{M}{y_o}\sin\theta$.

This shows that the locus of the zero-crossings of the phase difference matrix is a family of lines given by

$$\frac{\rho}{\cos\theta}x_o + \frac{\rho}{\sin\theta}y_o = k(M+N) \tag{13}$$

Each line itself is parameterized by the angle θ and its distance ρ from the center frequency (i.e. the origin of the frequency domain). This is an ideal setup for Hough transform, which maps these lines to a parameter space of (θ, ρ). As can be verified above, θ remains invariant among all lines and ρ varies as integer multiples of some other invariant parameter, i.e. $\rho = k\rho_o$. Therefore in the Hough-transform domain, we expect to see a set of peak values situated at equal distances from each other, and parallel to the ρ-axis. Figure 2 shows an example of the Hough transform of the discontinuities of the phase difference matrix of two shifted images, where the peaks can be clearly identified.

Each peak point in the Hough-transform domain provides one linear constraint on x_o and y_o. Given a total of t such peak values, we can construct a system of linear equations of the form

$$\mathbf{A}\mathbf{r} = \mathbf{b} \quad \text{where} \quad \mathbf{A} = \begin{bmatrix} \frac{\rho_1}{\cos\theta_1} & \frac{\rho_1}{\sin\theta_1} \\ \vdots & \vdots \\ \frac{\rho_t}{\cos\theta_t} & \frac{\rho_t}{\sin\theta_t} \end{bmatrix} \tag{14}$$

$\mathbf{r} = [x_o \;\; y_o]^T$, and $\mathbf{b} = (M+N)[k_1 \cdots k_t]^T$.

The norm-regularized solution [8] to this over-determined system of equations is given by

$$\mathbf{r}_{\text{opt}} = (\mathbf{A}^T\mathbf{A} + \lambda\mathbf{L}^T\mathbf{L})^{-1}\mathbf{A}^T\mathbf{b} \tag{15}$$

where λ is a regularization parameter, and $\mathbf{L}$ is such that

$$\mathbf{L}^T\mathbf{L} = \begin{bmatrix} 2 & -1 \\ -1 & 2 \end{bmatrix} \tag{16}$$

This choice of $\mathbf{L}$ [8] implies that our *a priori* belief is that our solution should be identical over all equations in the system, i.e. the equations should be consistent with each other. The optimal choice for the regularization parameter is given by the method of GCV, which amounts to minimizing

$$\text{GCV}(\lambda) = \frac{\|(\mathbf{I} - \mathbf{A}(\mathbf{A}^T\mathbf{A} + \lambda\mathbf{L}^T\mathbf{L})^{-1}\mathbf{A}^T)\mathbf{b}\|^2}{(\text{tr}(\mathbf{I} - \mathbf{A}(\mathbf{A}^T\mathbf{A} + \lambda\mathbf{L}^T\mathbf{L})^{-1}\mathbf{A}^T))^2} \tag{17}$$

with respect to λ, where tr$(\cdot)$ is the trace of a matrix. A first order approximation to the optimal value of λ is given by [2]:

$$\lambda^* = \frac{\sigma_1 \sum_{j=2}^{t} s_j^2}{(t-1)s_1^2 - \sum_{j=2}^{t} s_j^2} \tag{18}$$

where σ_1 is the dominant eigenvalue of $\mathbf{A}\mathbf{L}^{-1}\mathbf{L}^{-T}\mathbf{A}^T$, and s_j are the components of the vector $\mathbf{V}^T\mathbf{b} = [s_1 \; s_2 \; \ldots \; s_t]^T$, where $\mathbf{V}$ is the matrix of the eigenvectors of $\mathbf{A}\mathbf{L}^{-1}\mathbf{L}^{-T}\mathbf{A}^T$.

Using (15) and (18), we can compute the optimal solutions for x_o and y_o.

5 Results and Discussion

We applied our technique to a set of MRI data, used also by Hoge in his experimentation [3]. Figure 3 shows a pair of MRI images from this data set, and their phase difference matrix. The phase difference matrix is noisy and highly affected by aliasing. We repeated Hoge's exact experimental procedure. Table 1 summarizes the shift parameters obtained by our approach compared to those obtained by physical calibration, Stone et al. and Hoge. Similar to [3], we compared the different algorithms using the relative error. Results are shown in Fig. 5. Overall, given the very small variations of the relative error, the methods seem to be comparable in terms of performance. However, we found that our algorithm closely followed the physical calibration.

We then applied the method to estimate rotation and scaling in a log-polar sampling scheme, assuming known rotation center[3]. In log-polar sampling rotation and scaling reduce to simple translations, which can then be accurately

[2] The proof is omitted due to lack of space.

[3] Rotation center can be for instance identified by physical calibration.

estimated directly from the phase difference matrix as before. Figure 4 shows two MRI images with log-polar sampling and with rotation and scale differences. Their phase difference matrix shows clearly the sawtooth signal encoding the rotation and the scale as a sawtooth signal. Figure 4 shows the relative error for estimated rotation and scale for a wide range of added noise levels. We repeated this experimentation for a large range of rotation angles and scale variations and obtained similar results to the one shown in Figure 4.

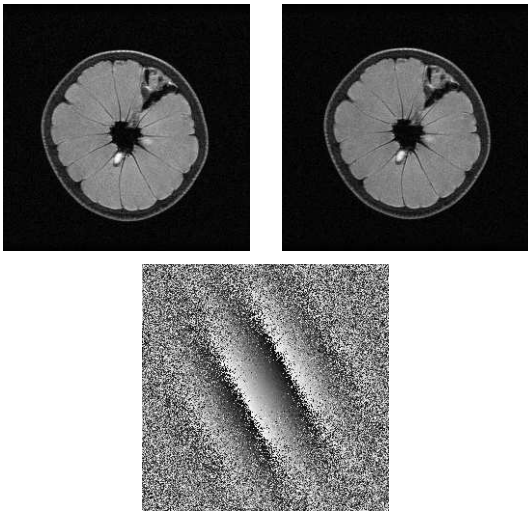

Figure 3. A pair of images from the MRI data set (Courtesy of W.S. Hoge), and their discrete phase difference matrix.

Image Pairs	Physical (in pixels)	Stone et al.	Hoge	Proposed Method
(1,2)	(-2.40, -4.00)	(-2.06,-5.97)	(-2.05,-4.02)	(-2.11,-4.00)
(1,3)	(-4.80,-8.00)	(-4.28,-9.99)	(-4.26,-8.01)	(-3.90,-7.49)
(1,4)	(-7.20,-4.32)	(-6.61,-5.67)	(-6.61,-4.33)	(-6.22,-3.93)
(1,5)	(-7.20,-12.00)	(-6.62,-13.97)	(-6.61,-12.03)	(-6.39,-11.42)
(2,3)	(-2.40,-4.00)	(-5.86,-3.85)	(-2.21,-3.98)	(-2.18,-3.87)
(2,4)	(-4.80,-0.32)	(-4.55, -1.71)	(-4.54,-0.32)	(-4.16,-0.31)
(2,5)	(-4.80,-8.00)	(-4.56,-10.00)	(-4.55,-8.01)	(-4.13,-7.73)
(3,4)	(-2.40,3.68)	(-2.34,2.34)	(-2.33,3.66)	(-2.34,3.55)
(3,5)	(-2.40,-4.00)	(-2.34,-5.97)	(-2.34,-4.03)	(-2.49,-3.83)
(4,5)	(0.00,-7.68)	(-0.81,-8.05)	(-0.01,-7.69)	(-0.03,-7.84)

Table 1. Pairwise registration of the MRI data set.

References

[1] E. De-Castro and C. Morandi. Registration of translated and rotated images using finite Fourier transforms. *IEEE Trans. PAMI*, vol. 9(no. 5):700–703, 1987.

[2] H. Foroosh, J. Zerubia, and M. Berthod. Extension of phase correlation to sub-pixel registration. *IEEE Trans. Image Processing*, vol. 11(3):pp. 188–200, 2002.

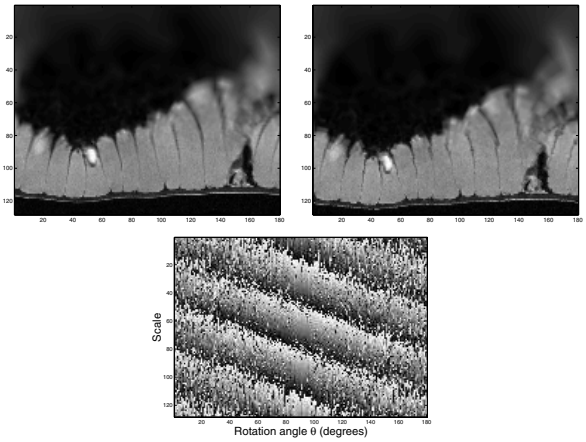

Figure 4. Log-polar samples of MRI images and their phase difference matrix.

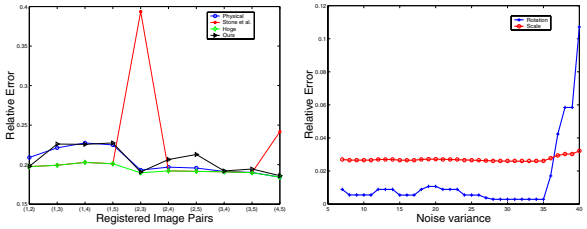

(a) (b)

Figure 5. (a) The relative error in estimated translations compared to the physical calibration, Stone et al., and Hoge, (b) The relative error in estimated rotation and scale versus noise variance.

[3] W. Hoge. Subspace identification extension to the phase correlation method. *IEEE Trans. Medical Imaging*, 22(2):277–280, 2003.

[4] P. Kostelec and S. Periaswami. Image registration for mri. *Modern Signal Processing*, 46:161–184, 2003.

[5] C. D. Kuglin and D. C. Hines. The phase correlation image alignment method. In *Proc. Int. Conf. on Cybernetics and Society*, pages 163–165, 1975.

[6] A. V. Oppenheim, R. W. Schafer, and with J.R. Buck. *Discrete-Time Signal Processing*. Prentice-Hall International Inc., 2nd edition, 1989.

[7] K. Scheffler. Tomographic imaging with nonuniform angular sampling. *Journal of Computer Assisted Tomography*, 23(1):162–166, 1999.

[8] A. Tikhonov and A. Arsenin. *Solutions of Ill-posed Problems*. Winston & Sons, 1977.

[9] A. Zemanian. *Distribution Theory and Transform Analysis*. Dover Publications Inc., 1965.